Using phase retrieval to measure the intensity and phase of ultrashort pulses: frequency-resolved optical gating

Rick Trebino

Combustion Research Facility, Sandia National Laboratories, Livermore, California 94551

Daniel J. Kane

Southwest Sciences, Inc., Suite E-11, 1570 Pacheco Street, Santa Fe, New Mexico 87501

We recently introduced a new technique, frequency-resolved optical gating (FROG), for directly determining the full intensity $I(t)$ and phase $\varphi(t)$ of a single femtosecond pulse. By using almost any instantaneous nonlinear-optical interaction of two replicas of the ultrashort pulse to be measured, FROG involves measuring the spectrum of the signal pulse as a function of the delay between the replicas. The resulting trace of intensity versus frequency and delay yields an intuitive display of the pulse that is similar to the pulse spectrogram, except that the gate is a function of the pulse to be measured. The problem of inverting the FROG trace to obtain the pulse intensity and phase can also be considered a complex two-dimensional phase-retrieval problem. As a result, the FROG trace yields, in principle, an essentially unique pulse intensity and phase. We show that this is also the case in practice. We present an iterative-Fourier-transform algorithm for inverting the FROG trace. The algorithm is unusual in its use of a novel constraint: the mathematical form of the signal field. Without the use of a support constraint, the algorithm performs quite well in practice, even for pulses with serious phase distortions and for experimental data with noise, although it occasionally stagnates when pulses with large intensity fluctuations are used.

1. INTRODUCTION

In the past 25 years the science and technology for the creation and use of ultrashort laser pulses have progressed tremendously. It is now possible to create laser pulses as short as a few femtoseconds in length,[1] and such pulses have found a wide range of applications.[2,3] Unfortunately, the means for measuring these pulses has not progressed so rapidly. What is sought is a technique for measuring the full, time-dependent intensity $I(t)$ and phase $\varphi(t)$, i.e., the full complex electric field $E(t)$ of an individual femtosecond pulse. For many years, however, only partial measures, such as the intensity autocorrelation, have been available.[4-6] Recently some progress in this search has been made,[7-28] although all techniques remain experimentally complex, and nearly all methods operate on a multishot basis only and continue to yield only partial information, such as the intensity but not the phase, or vice versa. The problem is difficult because durations of ultrashort pulses are much less than the temporal resolution of all available potential measuring devices. However, we recently developed an intuitive and general technique that achieves the measurement of the intensity and phase of an arbitrary femtosecond pulse by using a simple and novel experimental arrangement.[29-31] It also does so for a single laser pulse. The key to this development is the reduction of the problem to a complex two-dimensional phase-retrieval problem. It is our purpose in this paper to describe the technique briefly and then to treat in detail the iterative-Fourier-transform phase-retrieval algorithm that we use to obtain the pulse intensity and phase from the experimental trace. The algorithm is unique in that, whereas a support constraint is available, it uses instead an apparently more powerful constraint that follows from the known mathematical form of the signal function. This constraint results solely from knowledge of the nonlinear-optical interaction and involves no assumptions regarding the pulse. We show that the algorithm is quite robust, achieving convergence quickly in a wide range of cases. We also discuss important details of the algorithm's operation with theoretical and experimental examples.

2. FREQUENCY-RESOLVED OPTICAL GATING: BASIC CONCEPTS

Our pulse-measurement technique, which we call frequency-resolved optical gating (FROG),[29-31] requires splitting the pulse to be measured into two variably delayed replicas. The two pulse replicas are then crossed in any instantaneously responding nonlinear-optical medium. An optical-gate arrangement in an optical-Kerr medium, such as that shown in Fig. 1, is ideal. In this case the resulting signal-pulse electric field is given by

$$E_{\text{sig}}(t, \tau) \propto E(t)|E(t - \tau)|^2. \tag{1}$$

The spectrum of the signal pulse is then measured as a function of the delay between the two input pulses. The measured signal I_{FROG}, or FROG trace, is thus a function of frequency ω and delay τ:

$$I_{\text{FROG}}(\omega, \tau) \propto \left| \int_{-\infty}^{\infty} E_{\text{sig}}(t, \tau)\exp(-i\omega t)\mathrm{d}t \right|^2. \tag{2}$$

Such a measurement is easily made on a single-shot basis by focusing each beam with a cylindrical lens to a line

(a)

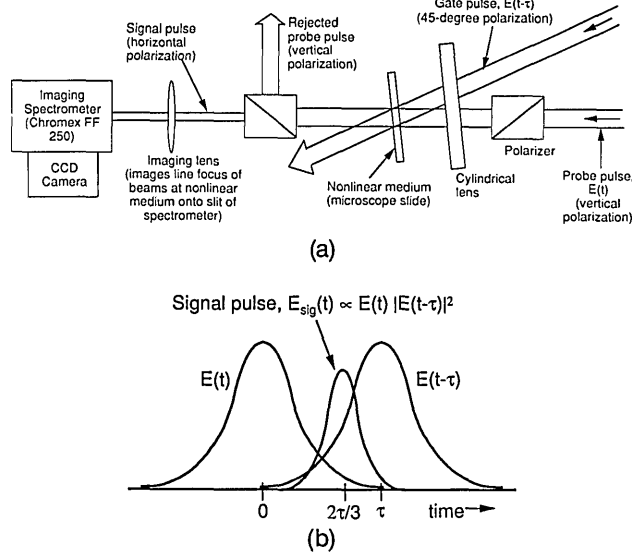Signal pulse, $E_{sig}(t) \propto E(t) |E(t-\tau)|^2$

(b)

Fig. 1. (a) FROG involves splitting the pulse and overlapping the two resulting pulse replicas $E(t)$ and $E(t - \tau)$ in an instantaneously responding nonlinear-optical medium. In this polarization-gating arrangement the probe pulse $E(t)$ passes through crossed polarizers and is gated at the nonlinear-optical sample medium by the gate pulse $E(t - \tau)$. The signal pulse is then spectrally resolved, and its intensity is measured versus frequency ω and delay τ. A single-shot beam geometry is shown here: each replica of the pulse is focused with a cylindrical lens to a line in the sample medium. A large beam angle is used so that delay varies spatially across the sample. The line focus at the sample medium is then imaged onto the entrance slit of the spectrometer with a spherical lens. Thus delay varies along the slit, and, after dispersion by the spectrometer, frequency varies along the dimension perpendicular to the slit. The FROG trace is the output intensity versus wavelength and delay as seen by the camera. (b) Schematic of the polarization-optical-gate FROG interaction of two Gaussian pulses. The signal pulse is also Gaussian and is centered at the time $2\tau/3$. Because the signal pulse's phase is contributed entirely by $E(t)$ [$E(t - \tau)$ appears as the squared magnitude], the signal pulse will reflect the instantaneous frequency of $E(t)$ at the time $2\tau/3$. For complex phase dependences, when the instantaneous frequency is an inappropriate description of the pulse phase, the signal pulse reflects the short-time spectrum of the probe pulse.

focus in the nonlinear-optical medium and imaging the signal beam onto the entrance slit of a spectrometer (see Fig. 1). Whether it is acquired on a single shot or many shots, the FROG trace can be considered a spectrogram[32-36] of the field $E(t)$:

$$S_E(\omega, \tau) \equiv \left| \int_{-\infty}^{\infty} E(t)g(t - \tau)\exp(-i\omega t)\mathrm{d}t \right|^2 \quad (3)$$

with variable-delay gate $g(t - \tau) = |E(t - \tau)|^2$. We will not utilize this fact, however, because inversion algorithms for spectrograms generally require knowledge of the gate function,[33] which we do not possess here. On the other hand, it is well known that the spectrogram is an extremely intuitive mathematical method for displaying a function. Indeed, the spectrogram of an acoustic wave is often used to display the acoustic wave, despite the availability of the actual pressure versus time data.[32] Analogously, we may conclude that the FROG trace is a similarly intuitive method for displaying an ultrashort pulse (see Figs. 2 and 3). And conveniently, for an ultrashort pulse, the FROG trace is directly and easily obtained experimen-

tally, as shown above, whereas the full intensity and phase are at present impossible to obtain directly.

3. FREQUENCY-RESOLVED OPTICAL GATING AS A COMPLEX TWO-DIMENSIONAL PHASE-RETRIEVAL PROBLEM

We now show that the full pulse field is essentially uniquely determined by the FROG trace, even for pathological pulse shapes and/or phases, by reducing the problem of inverting the FROG trace to a complex two-dimensional phase-retrieval problem. We first note that it is straightforward to obtain $E(t)$ from $E_{sig}(t, \tau)$ [this will be shown rigorously below; see relation (5)]. Thus, to solve the inversion problem, it is sufficient to be able to determine $E_{sig}(t, \tau)$ from the FROG trace. To do this we rewrite relation (2) in terms of $E_{sig}(t, \Omega)$, the one-dimensional Fourier transform of $E_{sig}(t, \tau)$ with regard to the delay variable τ. In terms of this new quantity we find that

$$I_{FROG}(\omega, \tau) \propto \left| \int_{-\infty}^{\infty} \int_{-\infty}^{\infty} E_{sig}(t, \Omega)\exp(-i\omega t - i\Omega\tau)\mathrm{d}t\mathrm{d}\Omega \right|^2, \quad (4)$$

which is indeed a two-dimensional phase-retrieval problem. At first glance, such a problem appears unsolvable because much information appears to be lost when the squared magnitude is taken. This is, of course, the case for one-dimensional phase-retrieval problems,[37] such as that of trying to find a light pulse's intensity and phase from its spectrum (a well-known unsolvable problem). Two- and higher-dimensional phase-retrieval problems, however, have been known for a decade to yield essentially unique results.[38-43] It is thus the case that unique solutions for $E_{sig}(t, \Omega)$ exist in essentially all cases. A constant phase factor and a translation in time remain ambiguous but are of no interest (see Appendix A). Thus, because $E(t)$ can be obtained easily from $E_{sig}(t, \Omega)$, we conclude that the FROG trace essentially uniquely determines the pulse intensity and phase.

In addition, phase-retrieval algorithms have been developed to find these solutions.[39,42-47] Unfortunately, solutions to the two-dimensional phase-retrieval problem can be difficult to find unless a sufficiently strong constraint exists to assist convergence.[43-45] Indeed, the complex version of this problem requires an even stronger constraint.[43,47] Support constraints are usually used in phase-retrieval problems, and a large body of literature exists describing the use of support constraints in phase retrieval of real positive images.[43-45] A few researchers have discussed the use of support constraints in complex phase-retrieval problems, finding that convergence occurs only in specific cases, such as when the support is confined to separate, nonoverlapping regions.[43,47] In FROG a support constraint can be obtained from the third-order intensity autocorrelation function $\int I(t)I^2(t - \tau)\mathrm{d}t$, which is obtained by computing $\int I_{FROG}(\omega, \tau)\mathrm{d}\omega$. We use, however, a different and, as we show below, more powerful contraint: the known mathematical form of the signal field $E_{sig}(t, \tau) \propto E(t)|E(t - \tau)|^2$, which yields the relation

$$E(t) \propto \int_{-\infty}^{\infty} E_{sig}(t, \tau)\mathrm{d}\tau, \quad (5)$$

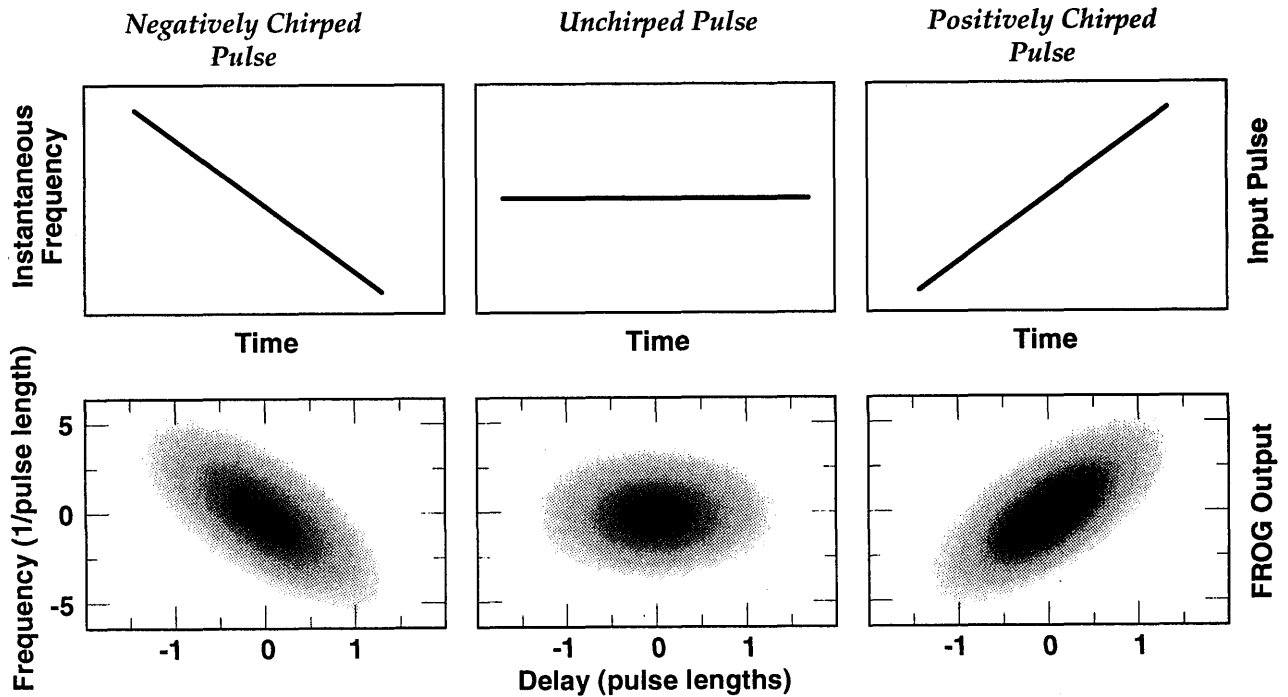where the proportionality constant is the reciprocal of the

Fig. 2.   FROG traces for negatively chirped, unchirped, and positively chirped Gaussian pulses.   The top figures show the instantaneous frequency versus delay curves for the pulses.   Note that the FROG trace reflects the instantaneous frequency of the pulse in all cases. Here the FROG traces are shown as density plots, with black indicating high intensity and white indicating low intensity.
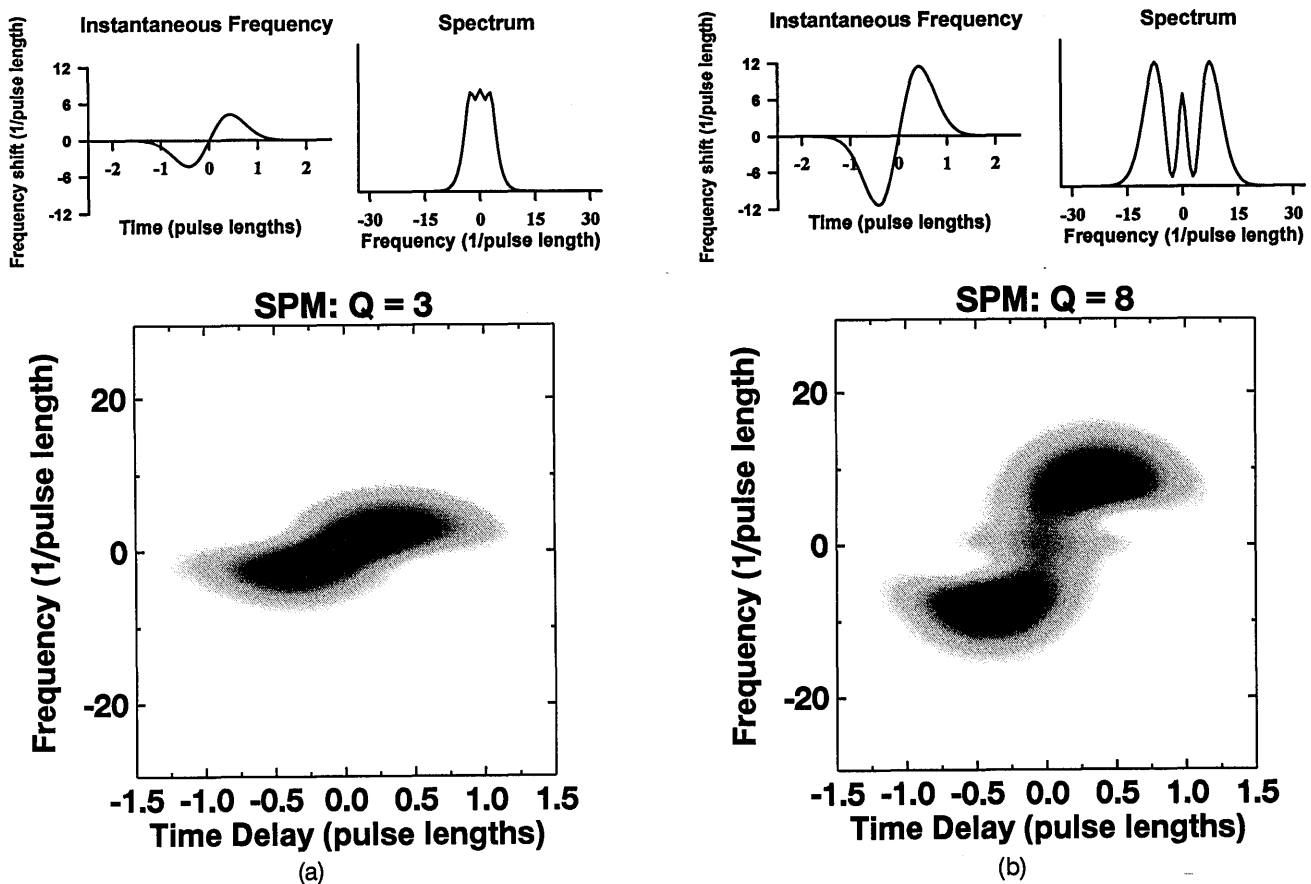

Fig. 3.   Theoretical instantaneous frequencies versus time, spectra, and FROG traces for self-phase-modulated pulses: (a) a weakly self-phase-modulated pulse ($Q = 3$), (b) a strongly self-phase-modulated pulse ($Q = 8$).   Note that for the weakly self-phase-modulated pulse the FROG trace visually displays the pulse's instantaneous frequency versus time.   For the strongly self-phase-modulated pulse the FROG trace also visually displays the pulse's instantaneous frequency versus time if the mean wavelength is computed for each delay. The additional structure in the latter trace indicates the breakup of the spectrum because of self-phase modulation (SPM).   Spectrograms of such pulses are similar to these traces when similar-length windows are used.

quantity $\int |E(\tau')|^2 d\tau'$, which is simply proportional to the pulse energy, a constant, independent of time. Thus an estimate for $E_{\text{sig}}(t, \tau)$ immediately gives an estimate for $E(t)$ by means of relation (5), which can then be used to give a new estimate for $E_{\text{sig}}(t, \tau)$ through relation (1). This process is convenient; it generates both the next-iteration value of the pulse field $E(t)$ and the next-iteration value of the signal field $E_{\text{sig}}(t, \tau)$ that satisfies the mathematical-form constraint.

We have implemented a simple iterative-Fourier-transform algorithm analogous to iterative-Fourier-transform algorithms that are used in image science.[43-45] We work with $E_{\text{sig}}(t, \tau)$ and one-dimensional Fourier transforms, however, rather than using a two-dimensional iterative-Fourier-transform routine with $E_{\text{sig}}(t, \Omega)$. The reason for this involves the constraint. In the two-dimensional case the above constraint would have to be written in terms of $E_{\text{sig}}(t, \Omega)$, and it would become $E(t) \propto E_{\text{sig}}(t, \Omega = 0)$. This two-dimensional implementation, however, would be wasteful in some sense because the constraint does not utilize the full two-dimensional field $E_{\text{sig}}(t, \Omega)$; it uses only the set of values with $\Omega = 0$. On the other hand, a one-dimensional Fourier-transform algorithm, in conjunction with the integration of relation (5), is equivalent to the two-dimensional implementation with the form of the constraint $E(t) \propto E_{\text{sig}}(t, \Omega = 0)$ because the integral of a function is its Fourier transform evaluated at zero. Thus one-dimensional Fourier transforms appear sufficient.

Like other iterative-Fourier-transform routines, ours involves Fourier transforming back and forth between domains. In our one-dimensional implementation we Fourier transform between $E_{\text{sig}}(t, \tau)$ and $E_{\text{sig}}(\omega, \tau)$ (see Fig. 4). As is also commonly done in iterative-Fourier-transform algorithms, in the ω domain we replace the magnitude of the kth iteration of the signal field with the square root of the data. Specifically, we replace the magnitude of $E_{\text{sig}}^{(k)}(\omega, \tau)$ with the square root of the measured FROG trace $I_{\text{FROG}}(\omega, \tau)$. In the t domain we use the above constraint.

Specifically, our implementation of the above constraint involves generating the $(k + 1)$st iteration for $E_{\text{sig}}(t, \tau)$ by first finding $E^{(k+1)}(t)$, the $(k + 1)$st iteration for $E(t)$, with the use of relation (5):

$$E^{(k+1)}(t) \equiv \int_{-\infty}^{\infty} E_{\text{sig}}^{(k)}(t, \tau) d\tau. \qquad (6)$$

We ignore the proportionality constant shown in relation (5) because we will normalize $E^{(k+1)}(t)$ at a later stage. Using relation (1), we then construct $E_{\text{sig}}^{(k+1)}(t, \tau)$, the $(k + 1)$st iteration for $E_{\text{sig}}(t, \tau)$:

$$E_{\text{sig}}^{(k+1)}(t, \tau) \equiv E^{(k+1)}(t)|E^{(k+1)}(t - \tau)|^2. \qquad (7)$$

Thus from $E_{\text{sig}}^{(k)}(t, \tau)$, the kth estimate for $E_{\text{sig}}(t, \tau)$, we have constructed a new estimate $E_{\text{sig}}^{(k+1)}(t, \tau)$, which is consistent with the mathematical form of the nonlinear-optical interaction. In addition, the $(k + 1)$st estimate for the pulse electric field, the desired quantity, is also provided by this process.

We have no proof of convergence of this algorithm. Indeed, we found that in practice both measures of the error that we define below can increase with increasing iteration

number, but in general the overriding tendency is for the error to decrease. However, it is important to note that the vast majority of practical phase-retrieval problems that are currently being solved by available algorithms lack convergence theorems. For example, one version of the iterative-Fourier-transform algorithm, the error-reduction version, has a convergence proof but performs much less effectively in practice than does another version, the hybrid-input–output version, for which no convergence proof exists.[43,45] Thus it is clear that the theoretical underpinnings of all these methods require additional attention, but what is important in practice is the performance of a technique rather than the existence of a convergence proof for the specific problem.

4. IMPLEMENTATION OF THE ITERATIVE-FOURIER-TRANSFORM ALGORITHM WITH MATHEMATICAL-FORM CONSTRAINT

We wrote a FORTRAN-77 program on a time-shared Silicon Graphics Indigo workstation that uses (Sandia public-domain) SLATEC fast-Fourier-transform subroutines. No attempt was made to optimize the code. The program requires ~1 s to perform each iteration for a FROG trace consisting of 125 × 125 elements. For the initial guess in the iteration we used a variety of pulse E fields, including a constant field, approximately correct fields, deliberately incorrect fields, and randomly generated noise for both the intensity and the phase of the pulse. Additional features of the program are discussed in Section 5.

To summarize, the program converged rapidly and reliably in all the cases that we tried, except when large intensity fluctuations occurred in the pulse. In the latter case it is not clear whether stagnation occurred because intensity fluctuations between points were too large (this problem can be solved by using a larger point density) or whether improvements must be made to the algorithm for complex pulse intensities. In either case a number of possible improvements are straightforward. In addition, when convergence occurred to the given FROG trace, the derived intensity and phase were always correct except for a constant multiplicative phase factor or a translation in time, the known trivial ambiguities (which are indeed trivial in this problem).

Specifically, the first case that we discuss is a squarish pulse, whose intensity is given by $I(t) \propto \exp(-t^4)$. We took this pulse to be positively linearly chirped, so that its phase was given by $\varphi(t) = -\alpha t^2$. The instantaneous frequency
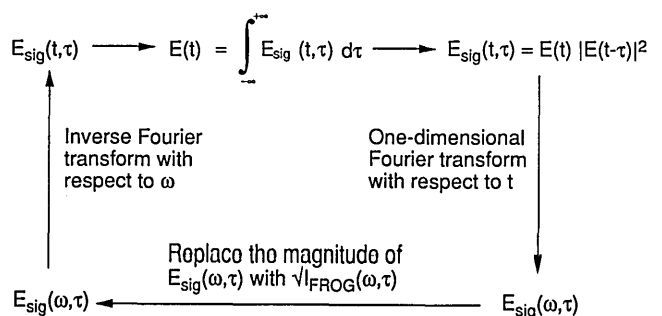

Fig. 4. Iterative-Fourier-transform algorithm for inverting a FROG trace to obtain an ultrashort pulse's intensity and phase.
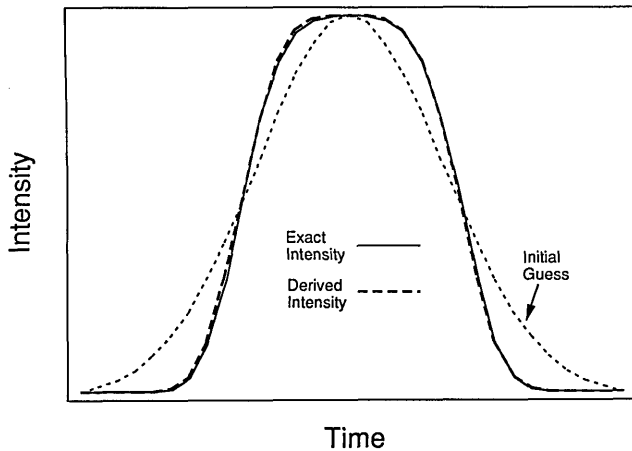
Fig. 5. Results of the algorithm after ten iterations for a squarish pulse: the exact pulse intensity, the initial guess intensity, and the derived pulse intensity.
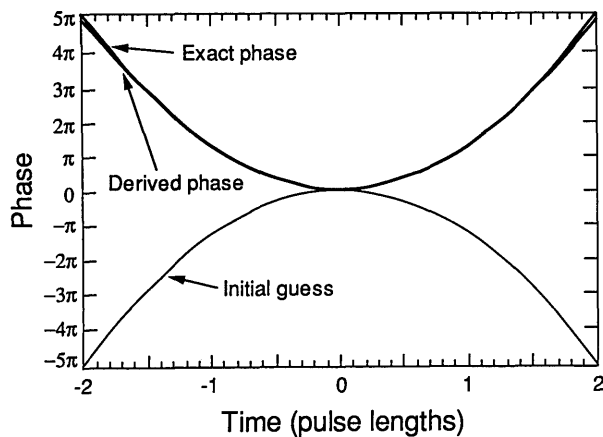

Fig. 6. Results of the algorithm after 20 iterations for a linearly chirped Gaussian pulse: the exact pulse phase, the initial guess phase, and the derived pulse phase.

of a field is given by $\omega(t) = -\mathrm{d}\varphi/\mathrm{d}t$, so this pulse's instantaneous frequency was $\omega(t) = 2\alpha t$. For this example we used $\alpha = 1$. This pulse models a commonly encountered ultrashort pulse resulting from propagation through a self-phase-modulating medium with group-velocity dispersion. Such a pulse is useful because, by use of a pair of diffraction gratings, it can be compressed essentially to the transform limit.[48] The FROG trace of such a pulse is approximately that of the positively chirped pulse shown in Fig. 2. For an initial guess to the algorithm for this pulse we used the correct phase but an incorrect intensity: a Gaussian intensity of approximately the correct width (see Fig. 5). We used $N = 33$, i.e., 33 temporal points defined the intensity versus time. At the steepest part of the pulse, intensity changes of ~20% occurred between adjacent points. Despite these large intensity changes, convergence to the correct intensity occurred rapidly, and the correct phase was maintained. Figure 5 shows the derived pulse intensity after ten iterations, where some deviations between the derived and exact pulses remain, but they are small and diminish rapidly with additional iterations.

In a second example we used the correct intensity but a deliberately incorrect phase. We took the exact pulse to have a Gaussian intensity and linear chirp with $\alpha = 1$.

As an initial guess we used linear chirp, but of the opposite sign, $\alpha = -1$, a particularly inaccurate initial guess. In the wings the exact pulse and the initial guess differed in phase by as much as 10π. With $N = 33$, again convergence occurred rapidly to the correct intensity and phase. Figure 6 shows the derived phase after 20 iterations, indicating excellent agreement. Interestingly, the derived phase in the wings of the pulse was quite accurate despite the low intensity there. In both these examples pulse E-field accuracy of better than 0.1% was achieved in <20 iterations.

The next two examples correspond to much more challenging problems. For our third example (see Fig. 7) we took the exact pulse to be a Gaussian-intensity pulse with a satellite pulse having 25% of the peak intensity of the main pulse (50% of the peak field strength of the main pulse) following it. In addition, we let the pulse phase be dominated by SPM. SPM (in its simplest manifestation) involves a phase $\varphi(t) = QI(t)$ so that $\omega(t) = -Q\mathrm{d}I/\mathrm{d}t$, where $I(t)$ is normalized to have unity peak magnitude.[49] The Q parameter is the measure of the strength of SPM. $Q \ll 1$ corresponds to a fairly weak effect, whereas $Q > \pi$ corresponds to a strong effect, which involves spectral breakup[49] (see Fig. 3). In this problem we allowed the exact pulse to have moderate
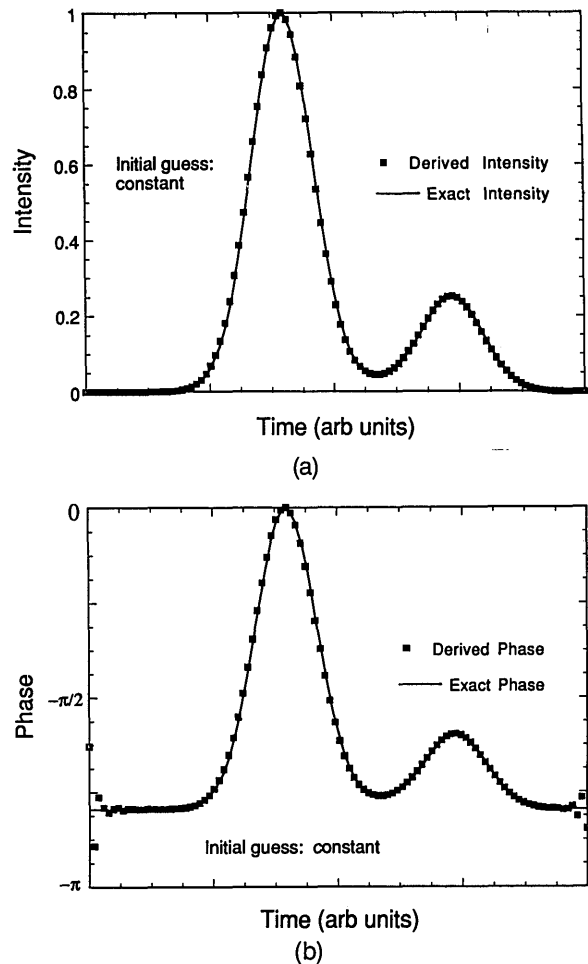

(a)

(b)

Fig. 7. Results of the algorithm for a Gaussian-intensity pulse with a trailing satellite pulse each with some SPM ($Q = 2.5$): (a) the exact pulse intensity and the derived pulse intensity, (b) the exact pulse phase and the derived pulse phase.
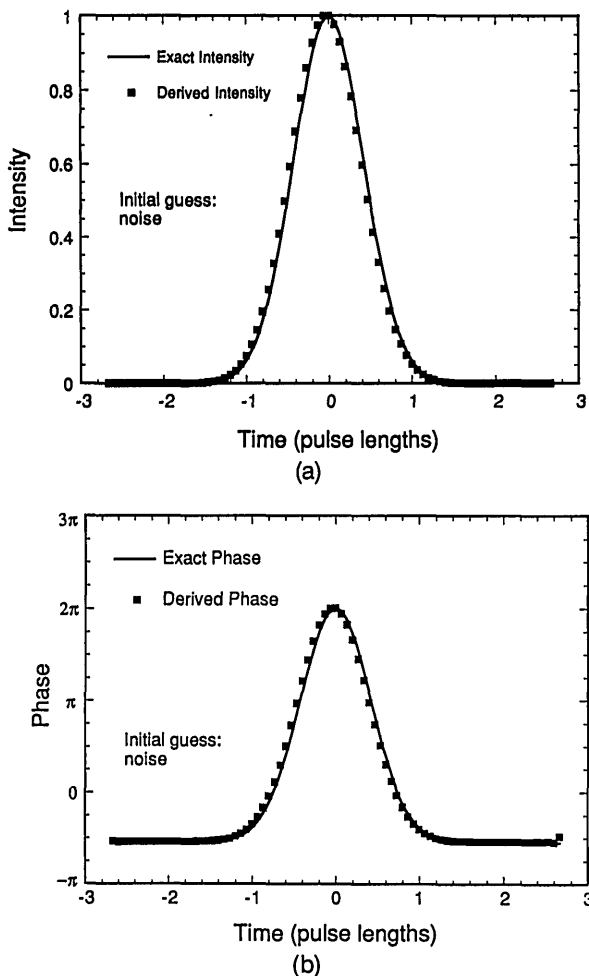
Fig. 8. Results of the algorithm for a severely self-phase-modulated Gaussian-intensity pulse ($Q = 8$): (a) the exact pulse intensity and the derived pulse intensity, (b) the exact pulse phase and the derived pulse phase.

SPM, at setting $Q = 2.5$. We set $N = 125$, used a FWHM for each pulse of 15 time increments, and separated the pulse centers by 35 time increments. At the steepest part of the pulse, intensity changes of ~10% occurred between adjacent points. For this problem we used an inaccurate initial guess: constant intensity and phase. Nevertheless convergence occurred to the correct intensity and phase (except, of course, in the extreme wings of the pulse, where the intensity is approximately zero and the phase is indeterminate).

Finally, to test the algorithm further, we used a difficult problem, a Gaussian-intensity pulse with severe SPM, with $Q = 8$, as a fourth example (shown in Fig. 3). We again set $N = 125$ and used a pulse-intensity FWHM of 15 time increments. In this case the phase of the pulse changed drastically between time increments in the steepest part of the pulse—by ~1 rad. In principle, a smaller time increment would be advised for such a run to reduce these phase jumps. For the initial guess in this case we used noise, i.e., random numbers for both the intensity (between 0 and 1) and phase (between $-\pi$ and π). Again convergence to the correct intensity and phase occurred, as is illustrated in Fig. 8.

We also tried pulses with significant variations in intensity, such as double pulsing, in which each pulse had the

same or nearly the same peak height. In such cases we found that the algorithm tended to stagnate, producing neither the correct FROG trace nor the correct intensity. Interestingly, the derived pulse in such cases was actually a double pulse, although the relative heights were wrong by an order-unity factor. It is also interesting that the phase was typically quite close to the exact result in all the cases that we tried. We believe that, when such stagnation occurs, examination of the pulse third-order intensity autocorrelation (obtainable directly from the FROG trace) should allow us to kick the E field in the correct direction. Other methods also exist, and we are currently working on this problem. However, femtosecond-pulse time–bandwidth products are not particularly large (laser amplifiers have limited bandwidth, and these pulses are extremely short), so we do not expect excessive intensity structure in such pulses. Indeed, it is generally believed that these pulses are more often plagued with slowly varying phase structure, describable with a fairly low-order polynomial expansion. In such cases our iterative-Fourier-transform algorithm performs quite well.

5. CONVERGENCE PROPERTIES OF THE ITERATIVE-FOURIER-TRANSFORM ALGORITHM WITH MATHEMATICAL-FORM CONSTRAINT

To discuss the convergence properties of the algorithm, we must first define appropriate measures of the error between the actual and derived E fields and the actual and derived FROG traces.

We define two measures of this error. For theoretical simulations, in which the actual pulse E field is known, an obvious measure of the error, which we will call the E-field (rms) error, is

$$\epsilon_E^{(k)} \equiv \left[\frac{1}{N} \sum_{j=1}^{N} |E^{(k)}(t_j) - E(t_j)|^2 \right]^{1/2}, \qquad (8)$$

where $E(t_j)$ is the exact E field at the time t_j, N is the number of points in the vector defining the E field, and t_j is the jth time in the time vector. $\epsilon_E^{(k)}$ is a measure of the accuracy of the derived pulse E field. It reveals phase as well as amplitude deviations in the derived pulse E field.

Another measure of the error between the exact and derived pulse fields that is useful in experimental situations when the exact pulse E field is unknown, as well as in theoretical simulations, and that we will call the FROG-trace (rms) error, is

$$\epsilon_{FROG}^{(k)} \equiv \left\{ \frac{1}{N^2} \sum_{i=1}^{N} \sum_{j=1}^{N} [I_{FROG}^{(k)}(\omega_i, \tau_j) - I_{FROG}(\omega_i, \tau_j)]^2 \right\}^{1/2}, \qquad (9)$$

where $I_{FROG}^{(k)}(\omega_i, \tau_j)$ is the kth iteration for the FROG trace, $I_{FROG}(\omega_i, \tau_j)$ is the measured FROG trace, and ω_i and τ_j are the ith frequency and the jth delay in the frequency and delay vectors, respectively.

A zero value for $\epsilon_E^{(k)}$ obviously guarantees a zero value for $\epsilon_{FROG}^{(k)}$, and the guaranteed uniqueness of the E field for a given FROG trace implies the converse. Nevertheless we treat the converse as a theory to be tested, at least initially.

In view of the trivial ambiguities, using these error measures requires that some normalizations and translations
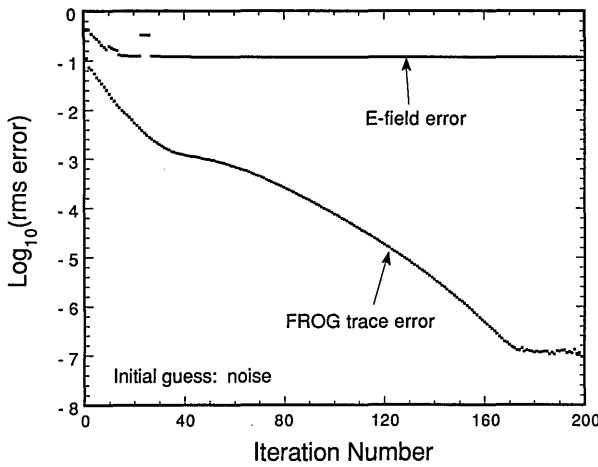
Fig. 9. Comparison of the two measures of error for the severely self-phase-modulated pulse. Note that the FROG-trace rms error decreases steadily, whereas the E-field rms error appears to stagnate. This occurs because the derived E field is slightly translated in time compared with the exact E field (see Fig. 8). In all the cases in which such discrepancies occurred we verified that the cause is this translation. In general, because the FROG trace essentially uniquely determines the E field, the FROG trace error is a more reliable measure of error than is the E-field error. (The discontinuities in the E-field error between iterations 20 and 30 are also the result of temporal translations.)

first be performed. For example, it will always be necessary to translate $E^{(k)}(t_j)$ appropriately and to normalize the derived E field by an appropriate complex constant to compute $\epsilon_E^{(k)}$ properly. As a result, in our computer program we translate both $E(t_j)$ and $E^{(k)}(t_j)$ so that their maxima occur at the central time ($j = N/2 + 1/2$; we use only odd values of N). We normalize $E(t_j)$ to have unity maximum, so that $\epsilon_E^{(k)}$ corresponds to the percentage error in $E(t)$ per point. We also normalize the derived pulse field on each iteration to minimize $\epsilon_E^{(k)}$. Normalizations are important for the measured and derived FROG traces as well. We normalize the measured $I_{FROG}(\omega_i, \tau_j)$ to have unity maximum, so that $\epsilon_{FROG}^{(k)}$ corresponds to the percentage error per unit point. Finally, for $\epsilon_{FROG}^{(k)}$ to make sense, we also normalize $I_{FROG}^{(k)}(\omega_i, \tau_j)$ on each iteration to minimize $\epsilon_{FROG}^{(k)}$. It is, of course, neither necessary nor appropriate to translate the exact or the derived FROG trace.

Translation of (i.e., centering) the E field proved useful for another reason. Before implementation of this feature the derived E field had a tendency to drift in time, apparently because nothing constrained it to remain in one place. This drift hindered convergence somewhat. (A support constraint could also have lessened this effect, although centering proved quite effective.)

For experimental runs we define convergence to mean $\epsilon_{FROG}^{(k)} < \eta$, where η is the percentage noise averaged over the data. Experimental runs that we performed typically had $\eta \approx 1\%$, and convergence occurred in 30–100 iterations for the approximately linearly chirped pulses we used.

For theoretical simulations we initially defined convergence to mean $\epsilon_E^{(k)} < 10^{-7}$. This value also corresponds roughly to the round-off error of single precision for the values of N that we used. Typically, however, the field error appeared to stagnate at a fairly large value (~1% to 10%), whereas the FROG-trace error achieved a very low value (10^{-7}), indicating convergence. Figure 9 shows the

values of these two measures of error for the highly self-phase-modulated pulse, which illustrates this point. This type of event is of concern because it could indicate the presence of a low-probability ambiguity, such as in the case of the spectrogram, in which the relative phase of well-separated pulses is ambiguous[33] (see Appendix A). Close examination of Fig. 8, however, shows that the derived pulse intensity and phase are simply translated in time by approximately one half of a time increment with respect to the exact pulse intensity and phase, despite our centering routine. Indeed, in all cases we found that this effect was present because the derived pulse peak occurred between adjacent time values, thus destroying the usefulness of $\epsilon_E^{(k)}$ as a measure of E-field error. As a result we were careful to verify that, in all the cases that we tried, a low value of $\epsilon_{FROG}^{(k)}$ yielded the correct E field although possibly translated slightly in time. In the future we plan to implement an improved pulse-centering routine, but this problem will probably always persist to some extent. For the present we conclude that $\epsilon_{FROG}^{(k)}$ is an appropriate error measure for theoretical simulations as well as for experimental runs. In any case, in practical usage the exact E field will be unknown, and $\epsilon_{FROG}^{(k)}$ will be the only available error measure (although an error could be defined in terms of how well the constraint is satisfied). Fortunately $\epsilon_{FROG}^{(k)}$ appears to be adequate in all cases.

In practice we found that convergence to the 10^{-7} level in simulations typically occurred in 100–200 iterations for slowly varying pulses. FROG-trace errors of the order of 1% were typically achieved in 10–20 iterations. Convergence occurred more slowly when the intensity changed rapidly and/or the quality of the initial guess was poor. Figure 10 shows the value of $\epsilon_{FROG}^{(k)}$ for the pulse-with-satellite example from Section 4. Observe that little or no progress was made in the first eight iterations, as might be expected from our deliberately bad choice of initial guess of constant intensity and phase for this rapidly varying (both in intensity and phase) pulse. Nevertheless, after this inauspicious beginning, the algorithm converged fairly rapidly. Interestingly, after iteration 20 or so, the error decreased approximately exponentially until round-off error became important.
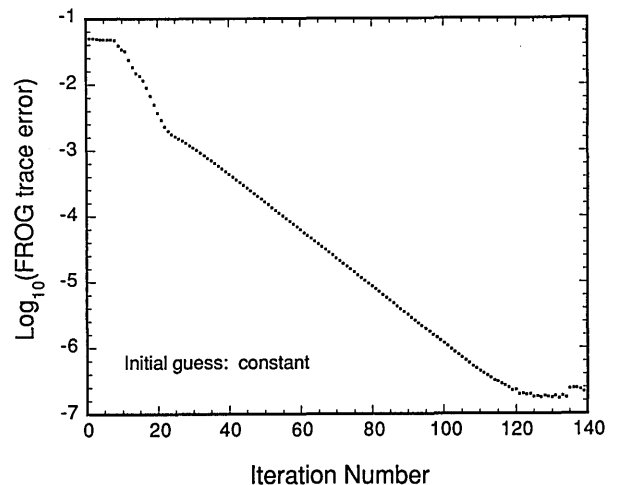

Fig. 10. Plot of the FROG-trace error for the iteration for the pulse with satellite and SPM.
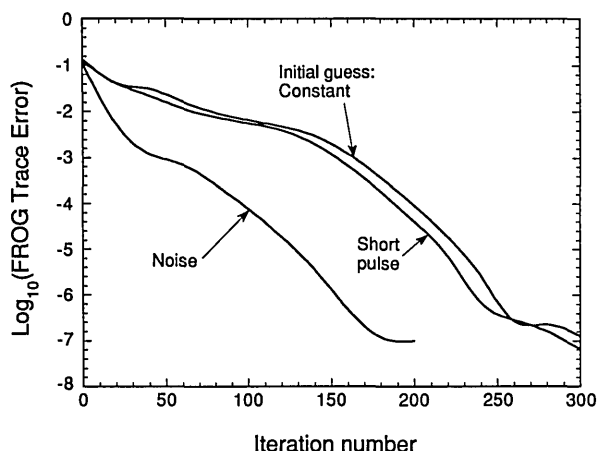
Fig. 11. Plot of FROG-trace rms error versus iteration number for the severely self-phase-modulated Gaussian-intensity pulse for various initial guesses. Observe that noise yields the fastest convergence.

We also studied the value of initial guesses in producing convergence. Figure 11 shows the FROG-trace error versus iteration number for the highly self-phase-modulated pulse from Section 4 with the use of three different types of initial guess. Specifically, we used constant intensity and phase, a short pulse of constant phase (with a pulse length that was slightly shorter than that of the actual pulse), and noise. We expected that the constant would be a poor initial guess, and it is, yielding slow convergence. Interestingly, the short pulse did no better. It is surprising that noise performed best, yielding convergence in about half the time that was required by the other types of initial guess. Noise performed well in other simulations that we ran, and only a highly accurate initial guess outperformed it. This result is in agreement with the performance of iterative-Fourier-transform routines that are used in image science, in which noise is the initial guess of choice.[45]

We also included in our program the possible use of a support constraint as well as the mathematical-form constraint. Whereas an automated procedure can be developed for determining the appropriate support from the FROG trace, as mentioned above, our implementation at this stage consisted simply of inputting a support for the pulse according to taste. We tried using both tight and loose support constraints but were not able to improve convergence in any case. Indeed, the use of a support constraint, in addition to the mathematical-form constraint, appeared to slow convergence on a few occasions. We also incorporated the hybrid-input–output form[45] of the support constraint and had similar experience with it. However, these statements should be considered preliminary at present because we have not fully evaluated this feature of the program.

The mathematical-form constraint was applied rigorously in all the cases. Some attempts were made to use an analogous version of this constraint incorporating the concept of a hybrid-input-output algorithm,[45] in which the constraint is not rigorously applied. In other words only some percentage of the change in the field indicated by the constraint is actually made in the field. Our implementation of this feature was as follows:

$$E^{(k+1)}(t) = \beta \left[C \int_{-\infty}^{\infty} E_{\text{sig}}^{(k)}(t, \tau) d\tau \right] + (1 - \beta) E^{(k)}(t), \quad (10)$$

where β is a parameter between 0 and 1 and C is a normalization constant that ensures that the two terms have equal maximum values before multiplication by the β-dependent factors. In our experience this also did not speed convergence, although this statement should be considered preliminary as well.

We also ran this algorithm on FROG traces with noise artificially included to test its robustness in more realistic situations. In these preliminary runs, even 10% (multiplicative) noise did not seriously alter the algorithm's ability to achieve convergence to the essentially correct pulse intensity and phase. We believe that this success is due to the averaging and smoothing effect of the constraint, which involves an integration [Eq. (6)]. Such averaging is not characteristic of other phase-retrieval problems. A more detailed discussion of FROG in the presence of noise is being prepared.

6. EXPERIMENT

Before we describe our experimental apparatus we must mention an additional requirement of the algorithm that especially pertains to its use with experimental data. Because of the use of the mathematical-form constraint, which mixes time and delay axes [see Eq. (7)], implementation of the iterative-Fourier-transform algorithm requires the use of a frequency spacing of the points of $\delta\nu = (N\delta\tau)^{-1}$, where N is the number of points per row and $\delta\tau$ is the delay increment. In view of this result it is important either to calibrate the scales in advance of the experiment or to rescale data before running the algorithm. In our experiments, typically an excess of spectral data was collected, and either spectral points were thrown away or a weighted average was taken of groups of points.

Our apparatus consisted of a cw-pumped, Rhodamine 6G, colliding-pulse mode-locked dye laser that produced pulses of <100 fs at a wavelength of 620 nm and a repetition rate of ~100 MHz and a 10-Hz Nd:YAG-pumped four-stage dye amplifier that amplified these pulses to an energy of ~200 μJ. Dispersion compensation using four SF-10 prisms could compress the resulting positively chirped ~300-fs pulses to ~100 fs. Spatial filtering produced a TEM_{00} beam, eliminating the need for performing a complex normalization of the experimental trace. A beam splitter and a neutral-density filter yielded two pulses of a few microjoules each. A cylindrical lens of ~1-m focal
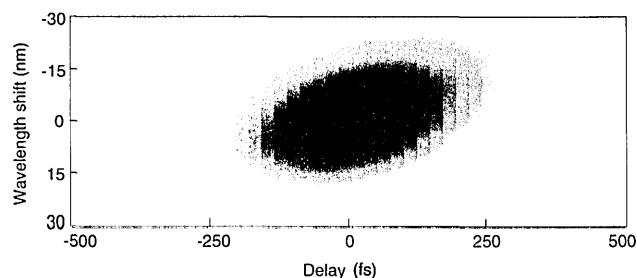

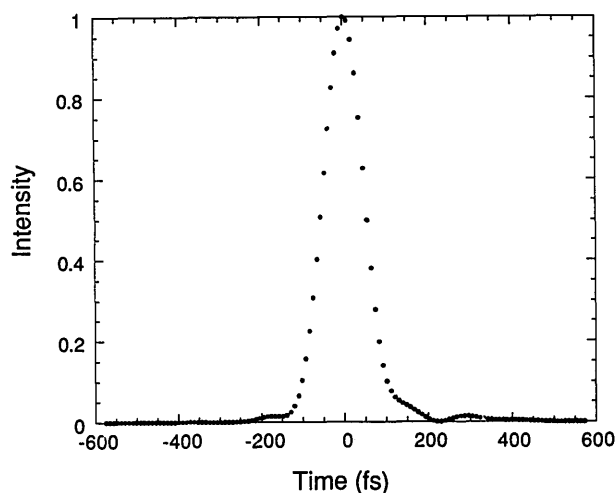Fig. 12. Experimental single-shot FROG trace for a linearly chirped pulse.

Fig. 13. Derived intensity evolution for the pulse whose FROG trace is shown in Fig. 12.
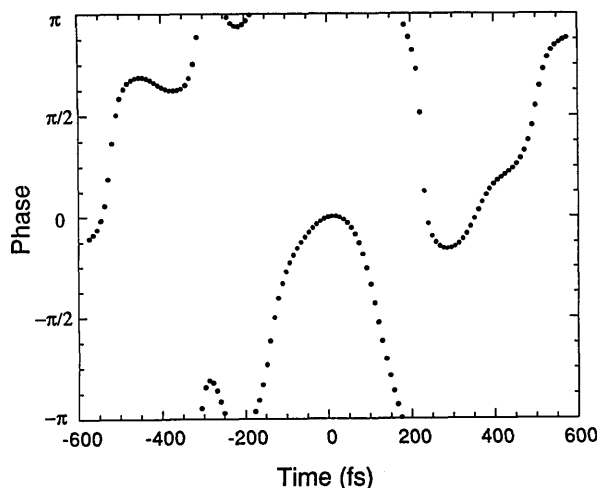

Fig. 14. Derived phase evolution for the pulse whose FROG trace is shown in Fig. 12. The inverted parabolic shape of the phase evolution indicates positive chirp, i.e., linearly increasing frequency versus time $[\omega(t) = -d\varphi/dt]$. (Phase behavior for large positive and large negative times is indeterminate because the intensity at these times is zero.)
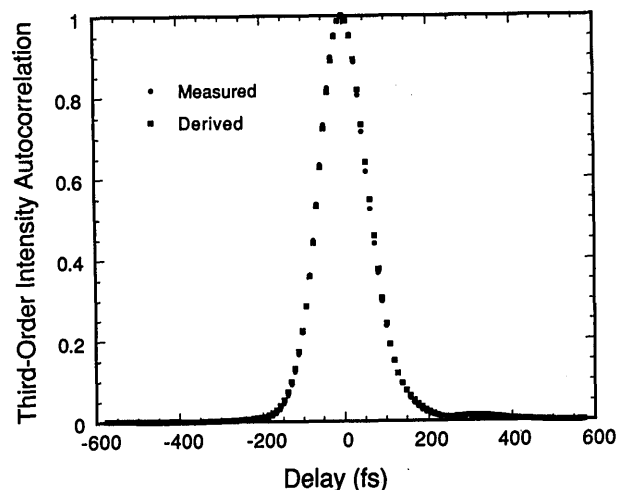

Fig. 15. Experimental and derived third-order intensity auto-correlation for the pulse of Figs. 12–14.

length focused the two beams, which crossed at an angle of ~20°, yielding a range of delays of ~1.2 ps. The electronic Kerr effect in a 3-mm-thick BK-7 window placed at the focus of these two beams provided signal light with ~10^{-4} efficiency. The peak intensity at the BK-7 was ~10 GW/cm² (an intensity for which we verified an approximately cubic dependence of diffracted energy versus input energy). We also observed negligible spectral broadening and small-scale self-focusing caused by the medium. We calculate that the effects of group-velocity dispersion resulting from the optics and sample medium were negligible at ~620 nm. The diffracted beam was focused onto the 50-μm slits of a 1/4-m Chomex imaging spectrometer. A Photometrics charge-coupled-device camera collected the dispersed light in a single shot. The signal intensity versus wavelength and delay, i.e., the FROG trace, was then recorded with a Macintosh IIci microcomputer.

Figure 12 shows the experimental FROG trace for a pulse that has been partially recompressed, which we expect to be somewhat positively linearly chirped (although less chirped than on emerging from the amplifier). Visual examination of the FROG trace easily reveals a pulse of the order of 100 fs in duration with a positive wavelength chirp (cf. Fig. 2) over the range of delays that we used. Indeed, use of the algorithm on the 125 × 125 array of data points yields a pulse ~110 fs (see Fig. 13) in length (FWHM) with an inverted parabolic phase evolution (see Fig. 14), indicative of a positive linear chirp, as discussed above. Noise was used as the initial guess for this iteration, and convergence occurred in 50 iterations. [As a result of the definition that we are using, convergence occurs more quickly when data are employed than in the simulations discussed above because the convergence condition here is determined by experimental noise rather than by computer round-off error and is necessarily less stringent: here the convergence condition is $\epsilon_{FROG}^{(k)} < $ ~1%. Actually we simply let the computer run and took the field that produced the lowest value of $\epsilon_{FROG}^{(k)}$. We found that in experimental runs the value of $\epsilon_{FROG}^{(k)}$ would reach a minimum and then begin to increase, oscillating up and down slightly above the best value. These oscillations rarely produced a better result, however.] The final value for $\epsilon_{FROG}^{(k)}$ for this data set was 0.5%, in reasonable agreement with the actual noise in the data. A check of these results is provided by Fig. 15, which shows the experimentally measured and the numerically derived third-order intensity autocorrelations for this pulse. The measured autocorrelation trace was obtained by integrating the measured FROG trace over frequency for each value of delay. This is not an ideal check of our derived results because it relies on data that are themselves used in the iteration; however, in view of the impossibility of measuring the pulse intensity and phase on a single shot in some other manner, it is reasonable.

We also measured longer pulses with some ringing in the trailing edge. For these pulses the algorithm converged quickly, and third-order autocorrelations indicate good fits in these cases also.

7. CONCLUSIONS

In conclusion, we have developed an iterative-Fourier-transform algorithm to extract the intensity and phase

evolution of a single ultrashort pulse from frequency-resolved optical-gating data. This algorithm is unique in its use of a constraint derived from the known mathematical form of the signal field that we obtained in the experiment. It makes no assumptions regarding the pulse field and is quite general. Theoretical simulations and experimental data reveal fairly robust performance for the algorithm, even for pulses with complex phase behavior or pulses in the presence of noise.

APPENDIX A: AMBIGUITIES IN FREQUENCY-RESOLVED-OPTICAL-GATING MEASUREMENTS

It is important to give a more rigorous discussion of the ambiguities in FROG measurements. Phase retrieval is known to possess trivial ambiguities. If $E_{sig}(x, y)$ is the correct solution, then additional ambiguous solutions can also result[43]:

(1) $E_{sig}(x, y) \exp(i\varphi_0)$, where φ_0 is a constant;
(2) $E_{sig}(x - x_0, y - y_0)$, where x_0 and y_0 are constants;
(3) $E_{sig}^*(-x, -y)$.

Despite their name, it is important to verify that these ambiguities lead in fact only to trivial and insignificant ambiguities in the pulse field. The first two ambiguities yield, respectively, an arbitrary constant phase factor and an arbitrary shift in time to the pulse field, which are of no concern in ultrashort-pulse measurement; i.e., they are not physically significant. The third ambiguity above is not consistent with the mathematical-form constraint and therefore cannot result.

Other ambiguities result only by chance, depending on the precise data, and are exceedingly unlikely.[38,40-43]

We should also mention that the spectrogram is known to have an additional ambiguity: the relative phase of well-separated pulses in a multiple-pulse field.[33] To see this let $S_E(\omega, \tau)$ be the spectrogram of the function $E(t)$. If $E(t) = E_1(t) + E_2(t)$, in which these two component fields are well separated in time (i.e., by much more than the window duration), then $S_E(\omega, \tau) = S_{E_1}(\omega, \tau) + S_{E_2}(\omega, \tau)$ because the cross terms are zero. Since the spectrogram is a squared magnitude, the relative phase of the two fields is ambiguous. FROG, on the other hand, has cross terms that are not present in the spectrogram because in FROG the gate is essentially the pulse itself and is always as broad in time as the pulse to be measured. Thus FROG avoids the only known physically significant ambiguity of the spectrogram.

Finally we should also mention that use of second-harmonic generation (SHG) as the FROG nonlinearity yields an ambiguity in the direction of time. To see this we write the SHG FROG signal as

$$I_{FROG}^{SHG}(\omega, \tau) = \left| \int_{-\infty}^{\infty} E(t)E(t - \tau)\exp(-i\omega t)dt \right|^2. \quad (A1)$$

Performing a simple change of variables, $t' = t - \tau$, and dropping the primes, we find that

$$I_{FROG}^{SHG}(\omega, \tau) = \left| \int_{-\infty}^{\infty} E(t)E(t + \tau)\exp(-i\omega t)dt \right|^2. \quad (A2)$$

Thus the SHG FROG signal is always symmetrical in the delay variable τ. As a result it will not be possible to distinguish the direction of time for the pulse. In addition, other ambiguities are likely to be present. Nevertheless, SHG FROG may have some applications. (Note: This appendix also appeared in Ref. 29, where we discussed FROG with the use of a different beam geometry and without the use of an iterative phase-retrieval algorithm.)

ACKNOWLEDGMENTS

REFERENCES AND NOTES

1. R. L. Fork, C. H. Brito-Cruz, P. C. Becker, and C. V. Shank, "Compression of optical pulses to six femtoseconds by using cubic phase compensation," Opt. Lett. **12**, 483–485 (1987).
2. H. L. Fragnito, J.-Y. Bigot, P. C. Becker, and C. V. Shank, "Evolution of the vibronic absorption spectrum in a molecule following impulsive excitation with a six fsec optical pulse," Chem. Phys. Lett. **160**, 101–104 (1989).
3. J. H. Glownia, J. A. Misewich, and P. P. Sorokin, "Femtosecond transition-state absorption spectroscopy of Bi atoms produced by photodissociation of gaseous Bi_2 molecules," J. Chem. Phys. **92**, 3335–3347 (1990).
4. E. P. Ippen and C. V. Shank, in *Ultrashort Light Pulses— Picosecond Techniques and Applications*, S. L. Shapiro, ed. (Springer-Verlag, Berlin, 1977), p. 83.
5. J. A. Giordmaine, P. M. Rentzepis, S. L. Shapiro, and K. W. Wecht, "Two-photon excitation of fluorescence by picosecond light pulses," Appl. Phys. Lett. **11**, 216–218 (1967).
6. N. G. Basov, V. É. Pozhar, and V. I. Pustovoit, "Measurement of the duration of high-power ultrashort optical pulses," Sov. J. Quantum Electron. **15**, 1429–1431 (1985).
7. J.-C. M. Diels, J. J. Fontaine, I. C. McMichael, and F. Simoni, "Control and measurement of ultrashort pulse shapes (in amplitude and phase) with femtosecond pulses," Appl. Opt. **24**, 1270–1282 (1985).
8. R. Trebino, C. C. Hayden, A. M. Johnson, W. M. Simpson, and A. M. Levine, "Chirp and self-phase modulation in induced-grating autocorrelation measurements of ultrashort pulses," Opt. Lett. **15**, 1079–1081 (1990).
9. J. T. Manassah, "Direct and second-harmonic interferometric determination of chirped pulse parameters," Appl. Opt. **26**, 2941–2942 (1987).
10. C. Yan and J. C. Diels, "Amplitude and phase recording of ultrashort pulses," J. Opt. Soc. Am. B **8**, 1259–1263 (1991).
11. K. Naganuma, K. Mogi, and H. Yamada, "General method for ultrashort light pulse chirp measurement," IEEE J. Quantum Electron. **25**, 1225–1233 (1989).
12. T. Kobayashi, F.-C Guo, A. Morimoto, T. Sueta, and Y. Cho, "Novel method of waveform evaluation of ultrashort optical pulses," in *Ultrafast Phenomena IV*, D. H. Auston and K. B. Eisenthal, eds. (Springer-Verlag, Berlin, 1984), pp. 93–95.
13. K. Naganuma, K. Mogi, and H. Yamada, "Time direction determination of asymmetric ultrashort optical pulses from second-harmonic generation autocorrelation signals," Appl. Phys. Lett. **54**, 1201–1202 (1989).
14. J. Jansky and G. Corradi, "Full intensity profile analysis of ultrashort laser pulses using four-wave mixing or third-harmonic generation," Opt. Commun. **60**, 251–256 (1986).
15. N. G. Paulter and A. K. Majumdar, "A new triple correlator design for the measurement of ultrashort pulses," Opt. Commun. **81**, 95–100 (1991).
16. A. S. L. Gomes, V. L. da Silva, and J. R. Taylor, "Direct measurement of nonlinear frequency chirp of Raman radiation in single-mode optical fibers using a spectral window method," J. Opt. Soc. Am. B **5**, 373–379 (1988).

17. G. Szabo, A. Müller, and Z. Bor, "A sensitive single-shot method to determine duration and chirp of ultrashort pulses with a streak camera," Opt. Commun. **82**, 56–62 (1991).

18. J. E. Rothenberg and D. Grischkowsky, "Measurement of optical phase with subpicosecond resolution by time-domain interferometry," Opt. Lett. **12**, 99–101 (1987).

19. T. F. Albrecht, K. Seibert, and H. Kurz, "Chirp measurement of large-bandwidth femtosecond optical pulses using two-photon absorption," Opt. Commun. **84**, 223–227 (1991).

20. K. W. DeLong and J. Yumoto, "Chirped light and its characterization using the cross-correlation technique," J. Opt. Soc. Am. B **9**, 1593–1604 (1992).

21. J. L. A. Chilla and O. E. Martinez, "Direct determination of the amplitude and the phase of femtosecond light pulses," Opt. Lett. **16**, 39–41 (1991).

22. J. L. A. Chilla and O. E. Martinez, "Frequency-domain phase measurement of ultrashort light pulses. Effect of noise," Opt. Commun. **89**, 434–440 (1992).

23. J. L. A. Chilla and O. E. Martinez, "Analysis of a method of phase measurement of ultrashort pulses in the frequency domain," IEEE J. Quantum Electron. **27**, 1228–1235 (1991).

24. A. Brun, P. Georges, G. Le Saux, and F. Salin, "Single-shot characterization of ultrashort light pulses," Rev. Sci. Instrum. **27**, 1225–1233 (1992).

25. E. P. Ippen and C. V. Shank, "Dynamic spectroscopy and subpicosecond pulse compression," Appl. Phys. Lett. **27**, 488–490 (1975).

26. J. P. Heritage, A. M. Weiner, and R. N. Thurston, "Fourier-transform picosecond pulse shaping and spectral-phase measurement in a grating pulse compressor," in *Ultrafast Phenomena V*, G. R. Fleming and A. E. Siegman, eds. (Springer-Verlag, Berlin, 1986), pp. 34–37.

27. A. M. Weiner, D. E. Leaird, J. S. Patel, and J. R. Wullert, "Programmable femtosecond pulse shaping by use of a multi-element liquid-crystal phase modulator," Opt. Lett. **15**, 326–328 (1990).

28. J. P. Foing, L. P. Likforman, and M. Joffre, "Femtosecond pulse phase measurement by spectrally resolved up-conversion," in *Ultrafast Phenomena VIII*, J. L. Martin and A. Migus, eds. (Springer-Verlag, to be published).

29. D. J. Kane and R. Trebino, "Characterization of arbitrary femtosecond pulses using frequency-resolved optical gating," J. Quantum Electron. **29**, 571–579 (1993). This paper also contains the proof of uniqueness of the FROG-trace inversion, but for the nonlinear-optical interaction of self-diffraction.

30. D. J. Kane and R. Trebino, "Single-shot measurement of the intensity and phase of a femtosecond pulse," in *Ultrafast Phenomena IX*, J. L. Martin and A. Migus, eds. (Springer-Verlag, to be published).

31. D. J. Kane and R. Trebino, "Single-shot measurement of the intensity and phase of an arbitrary femtosecond pulse using frequency-resolved optical gating," Opt. Lett. (to be published).

32. W. Koenig, H. K. Dunn, and L. Y. Lacy, "The sound spectrograph," J. Acoust. Soc. Am. **18**, 19–49 (1946).

33. S. H. Nawab, T. F. Quatieri, and J. S. Lim, "Signal reconstruction from short-time Fourier transform magnitude," IEEE Trans. Acoust. Speech Signal Process. **ASSP-31**, 986–998 (1983).

34. R. A. Altes, "Detection, estimation, and classification with spectrograms," J. Acoust. Soc. Am. **67**, 1232–1246 (1980).

35. L. Cohen, "Time-frequency distributions–a review," Proc. IEEE **77**, 941–981 (1989).

36. We note here, as in Ref. 29, that the spectrogram is not considered to be the ideal time- and frequency-resolved quantity. The Wigner distribution and wavelet transform, for example, are much more popular at the moment. [See, e.g., C. E. Heil and D. F. Walnut, "Continuous and discrete wavelet transforms," SIAM Rev. **31**, 628–666 (1989).] In our opinion, however, it is the spectrogram, or more precisely the FROG trace, that is the most easily experimentally measured time- and frequency-resolved quantity for ultrashort pulses. The above-mentioned alternative measures require such quantities as a time-reversed replica of the pulse or a variable-frequency and simultaneously variable-length window. Such quantities are quite difficult to obtain optically. On the other hand, the spectrogram's main inadequacy is that its fixed-length window cannot simultaneously provide good measurements of both long-term and short-term variations. This is not a problem for ultrashort-pulse measurement, in which the variations of interest are all short term. It may also be the case that, because in FROG the gate has exactly those time scales as the pulse, FROG may actually avoid the above problem in general, but we have not investigated this issue as yet.

37. E. J. Akutowicz, "On the determination of the phase of a Fourier signal. I," Trans. Am. Math. Soc. **83**, 234–239 (1956).

38. H. Stark, *Image Recovery: Theory and Application* (Academic, Orlando, Fla., 1987).

39. R. P. Millane, "Phase retrieval in crystallography and optics," J. Opt. Soc. Am. A **7**, 394–411 (1990).

40. R. Barakat and G. Newsam, "Necessary conditions for a unique solution to two-dimensional phase recovery," J. Math. Phys. **25**, 3190–3193 (1984).

41. R. G. Lane, W. R. Fright, and R. H. T. Bates, "Direct phase retrieval," IEEE Trans. Acoust. Speech Signal Process. **ASSP-35**, 520–525 (1987).

42. D. Israelevitz and J. S. Lim, "A new direct algorithm for image reconstruction from Fourier transform magnitude," IEEE Trans. Acoust. Speech Signal Process. **ASSP-35**, 511–519 (1987).

43. J. R. Fienup, "Reconstruction of a complex-valued object from the modulus of its Fourier transform using a support constraint," J. Opt. Soc. Am. A **4**, 118–123 (1987).

44. J. H. Seldin and J. R. Fienup, "Iterative blind deconvolution algorithm applied to phase retrieval," J. Opt. Soc. Am. A **7**, 428–433 (1990).

45. J. R. Fienup, "Phase retrieval algorithms: a comparison," Appl. Opt. **21**, 2758–2769 (1982).

46. R. G. Lane, "Phase retrieval using conjugate gradient minimization," J. Mod. Opt. **38**, 1797–1813 (1991).

47. R. H. T. Bates and D. G. H. Tan, "Fourier phase retrieval when the image is complex," in *Inverse Optics II*, A. J. Devaney and R. H. T. Bates, eds., Proc. Soc. Photo-Opt. Instrum. Eng. **558**, 54–59 (1985).

48. A. M. Johnson and C. V. Shank, "Pulse compression in single-mode fibers—picoseconds to femtoseconds," in *The Supercontinuum Laser Source*, R. R. Alfano, ed. (Springer-Verlag, New York, 1989). pp. 399–450.

49. Y. R. Shen and G.-Z. Yang, "Theory of self-phase modulation and spectral broadening," in *The Supercontinuum Laser Source*, R. R. Alfano, ed. (Springer-Verlag, New York, 1989), pp. 1–32.